

Review

Fluorescent Protein-Based Metal Biosensors

Ki Hyun Nam ^{1,2} 

¹ Department of Life Science, Pohang University of Science and Technology, Pohang 37673, Republic of Korea; structures@postech.ac.kr

² POSTECH Biotech Center, Pohang University of Science and Technology, Pohang 37673, Republic of Korea

Abstract: Fluorescent proteins (FPs) are optical probes that are used to track the functions of genetically encoded target molecules in molecular and cellular biology. FPs have intrinsic photophysical properties generated by the chromophore and its surrounding amino acid sequences. The intensity of the fluorescence emission of FPs can be changed using external factors such as pH or metal ions. Additionally, the fluorescence intensity of FPs can be reduced or quenched using specific transition metal ions, suggesting that they are attractive probes for measuring metal ion levels. A spectroscopical analysis of the metal-induced fluorescence quenching of several FPs revealed that they exhibited intrinsic fluorescence quenching behavior with specific metal ions. The quenchable metal-binding site of FP has been determined using chemical modification, crystal structure, and modeling, providing insights into the molecular mechanism and FP engineering. In this review, studies on the change in the fluorescence activity of FPs mediated by metal ions are comprehensively compared and reviewed, and the requirements for the development of fluorescent protein-based metal biosensors in the future are discussed.

Keywords: fluorescent protein; fluorescent quenching; FP; metal; biosensor



Citation: Nam, K.H. Fluorescent Protein-Based Metal Biosensors. *Chemosensors* **2023**, *11*, 216. <https://doi.org/10.3390/chemosensors11040216>

Academic Editors: Lintao Zeng and Minhuan Lan

Received: 27 February 2023

Revised: 27 March 2023

Accepted: 29 March 2023

Published: 30 March 2023



Copyright: © 2023 by the author. Licensee MDPI, Basel, Switzerland. This article is an open access article distributed under the terms and conditions of the Creative Commons Attribution (CC BY) license (<https://creativecommons.org/licenses/by/4.0/>).

1. Introduction

Metal ions are essential for all living organisms and play critical roles in fundamental biological processes such as osmotic regulation, catalysis, metabolism, biomineralization, and cell signaling [1]. Lack of essential metal ions in an organism can cause growth disorders, severe disruption in body functions, carcinogenesis, or death [2]. Moreover, a deficiency or excess of metal ions in living organisms can cause health problems, and their concentrations must be maintained within appropriate ranges for optimal cellular function [3–6]. Therefore, investigating the distribution and concentration fluctuations in metal ions within a cell can provide valuable insights for medical diagnoses related to cell signaling, metabolic engineering, or disease tracking [7,8].

Transition metal ions such as Cu, Ni, and Zn are involved in several physiological and pathophysiological pathways [9]. Several spectrophotometric and electroanalytical techniques, such as atomic absorption/emission spectroscopy [10,11], inductively coupled plasma mass spectroscopy [12–14], electrochemical assays [15,16], and colorimetric methods [17,18], have been widely used and have provided reliable results. However, these methods have several limitations in terms of expensive equipment, complex preprocessing, detection speed, and immediate detection in the field [7]. Therefore, the development of more accessible metal-detection probes is required. Among the various potential probe materials, fluorescent probes are attractive for metal detection because of their promising photophysical properties such as high sensitivity and selectivity, low detection limit, fast response, operational simplicity, real-time monitoring, and low cost [7,19].

In the field of biology, various biomolecules, such as peptides [20], enzymes [21], antibodies [22], nucleic acids [23], DNAzymes [24], and whole cells [25], are being developed as metal biosensors to measure metal ion levels. Fluorescent proteins (FPs) have photophysical properties because they emit fluorescence when the light of a specific wavelength is

absorbed [26–29]. FPs are widely used as optical probes to track the location and function of genetically encoded target molecules in various molecular and cell biology techniques, such as Förster or fluorescence resonance energy transfer (FRET) [30–32], biosensors [33–37], optogenetics [38–40], chemogenetics [41,42], subcellular localization [43–45], in vivo imaging [46–48], or genome editing [49–52] (Table 1).

Table 1. Application of fluorescent proteins in biological research.

Application	Biological Research	Reference
Förster or fluorescence resonance energy transfer (FRET)	Protein-protein interactions or conformational changes within proteins	[30–32]
Biosensors	Monitoring of small biomolecules or other physiological intracellular processes	[33–37]
Optogenetics	Measuring or controlling molecular signals, cells, or groups of cells	[38–40]
Chemogenetics	Monitoring cellular receptors that affect signal pathways within a cell	[41,42]
Subcellular localization	Monitoring the location of the target molecule in cells	[43–45]
In vivo imaging	Imaging plasmids or protein-protein interactions in organs	[46–48]
Genome editing	Monitoring genome editing	[49–52]

Green fluorescent protein (GFP) was first discovered in jellyfish (*Aequorea victoria*) [53]. GFP-like proteins form a β -can fold comprising an 11-stranded β -sheet [54]. A peptide portion penetrates the β -barrel, and the center of the β -barrel contains a chromophore composed of a tripeptide (Figure 1).

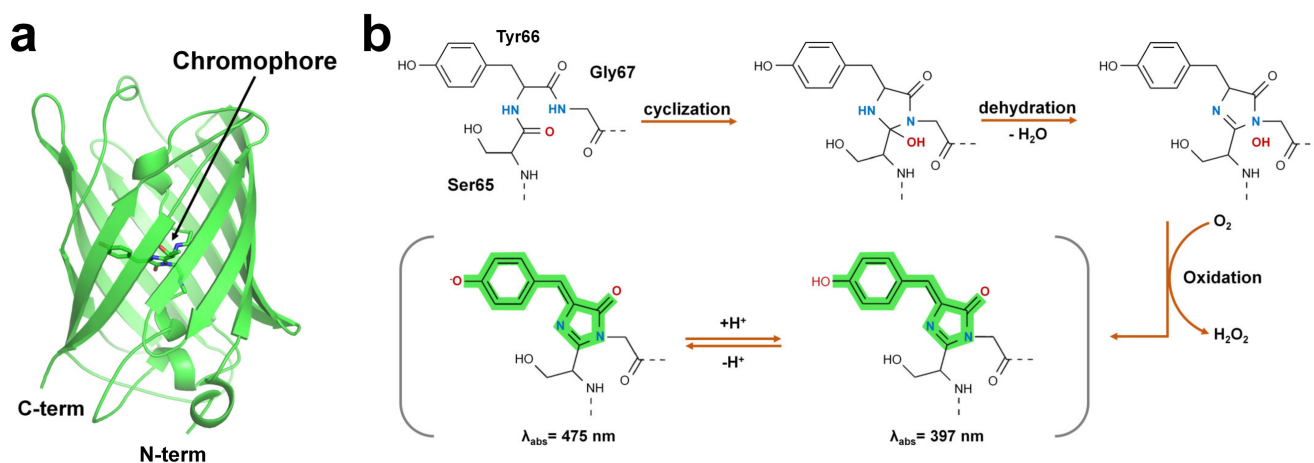


Figure 1. Structure of green fluorescent protein and chromophore. (a) Crystal structure of the green fluorescent protein (GFP) from jellyfish (PDB code: 1EMA). (b) GFP chromophore formation following a three-step autocatalytic process including cyclization, dehydration, and oxidation of three amino acids (Ser65, Tyr66, Gly67). Absorption properties of GFP are dependent on chromophore protonation states resulting in two absorption maxima in the excitation spectrum (the image concept was inspired from [37] and modified).

The FP chromophore is generated by post-translational modifications through processes such as folding, cyclization, dehydration, and oxidation [26] (Figure 1b). The chromophore of FP includes two or more ring structures, which are the most important sites for the optical properties of fluorescent proteins [55]. The quantum efficiency and absorption and emission wavelengths of FPs are affected by the constituting amino acids of the chromophore and the microenvironment surrounding the chromophore [26,55]. In addition, hydrogen bonds around the chromophore of FPs or bridges with water molecules

are formed, and the amino acids surrounding the chromophore are involved in determining the unique optical properties of FPs [27,28,56]. According to their absorption and emission wavelengths, FPs can be classified into blue/UV, cyan-green, yellow, orange, red, and far-red colors (Table 2).

Table 2. Classification of fluorescent proteins based on the fluorescence emission wavelength.

Color	Protein	λ_{Ex} (nm)	λ_{Em} (nm)	QY	Oligomerization	Reference
Blue/UV	Sirius	355	424	0.24	Monomer	[57]
	Azurite	383	447	0.55	Weak dimer	[58]
	moxBFP	385	448	0.56	Monomer	[59]
Cyan	Aquamarine	430	474	0.89	Monomer	[60]
	Cerulean	433	475	0.62	Weak dimer	[61]
	CyPet	435	477	0.51	Weak dimer	[62]
Green	mTurquoise2	434	474	0.93	Monomer	[63]
	mEGFP	488	507	0.60	Monomer	[64]
	mClover3	506	518	0.78	Monomer	[65]
Yellow	mNeonGreen	506	517	0.80	Monomer	[66]
	mGold	515	530	0.64	Monomer	[67]
	mCitrine	516	529	0.74	Monomer	[64]
Orange	mVenus	515	527	0.64	Monomer	[68]
	mOrange	548	562	0.69	Monomer	[69]
	mKO2	551	565	0.62	Monomer	[70]
Red	TurboRFP	553	574	0.67	Dimer	[71]
	tdTomato	554	581	0.69	Tandem dimer	[69]
	mApple	568	592	0.49	Monomer	[72]
Far-Red	mScarlet	569	594	0.70	Monomer	[73]
	mCherry	587	610	0.22	Monomer	[69]
	DsRed2	561	587	0.55	Tetramer	[74]
Far-Red	mPlum	590	649	0.10	Monomer	[75]
	mRaspberry	598	625	0.15	Monomer	[75]
	mNeptune	600	650	0.20	Monomer	[76]
	TagRFP657	611	657	0.10	Monomer	[77]

Values for optical properties were obtained from FPbase [78] (<https://www.fpbases.org/> (accessed on 1 February 2023)).

Moreover, based on their unique optical properties and applications, FPs can be classified into large Stokes shifts, photoactivatable, photoswitchable, and photoconvertible FPs (Table 3).

Table 3. Classification of fluorescent proteins based on optical properties.

Property	Protein	λ_{Ex} (nm)	λ_{Em} (nm)	QY	Brightness	Oligomerization	Ref.
Large Stokes Shift	tKeima	440	616	0.22	3.19	Tetramer	[79]
	LSSmKate2	460	605	0.17	4.42	Monomer	[80]
	T-sapphire	399	511	0.60	26.4	Weak dimer	[81]
Photoactivatable	PAmKate	586	628	0.18	4.5	Monomer	[82]
	PAmCherry1	564	595	0.46	8.28	Monomer	[83]
	PATagRFP	562	595	0.38	25.08	Monomer	[84]

Table 3. Cont.

Property	Protein	λ_{Ex} (nm)	λ_{Em} (nm)	QY	Brightness	Oligomerization	Ref.	
Photoswitchable	Dronpa	503	518	0.85	80.75	Monomer	[85]	
	mGeos-M	503	514	0.85	43.86	Monomer	[86]	
	rsTagRFP	567	585	0.11	4.05	Monomer	[87]	
Photoconvertible	Kaede	Green	508	518	0.88	86.94	Tetramer	[88]
		Red	572	580	0.33	19.93		
	mEos3.2	Green	507	516	0.84	53.26	Monomer	[89]
		Red	572	580	0.55	17.71		
	Dendra	Green	492	508	0.65	58.5	Tetramer	[90]
		Red	557	575	0.68	23.8		

Values for optical properties were obtained from FPbase [78] (<https://www.fpbase.org/> (accessed on 1 February 2023)).

All FP exhibit unique and intrinsic fluorescence properties. However, these properties are altered by various external environments. Accordingly, FPs have been suggested as biosensors for intracellular calcium indicators [91], chloride indicators [34], pH indicators [36,56], and ligand monitoring of receptors [33]. In particular, FPs are characterized by fluorescence quenching when exposed to a specific metal ion (Figure 2) and can potentially be used as an attractive probe for metal biosensors.

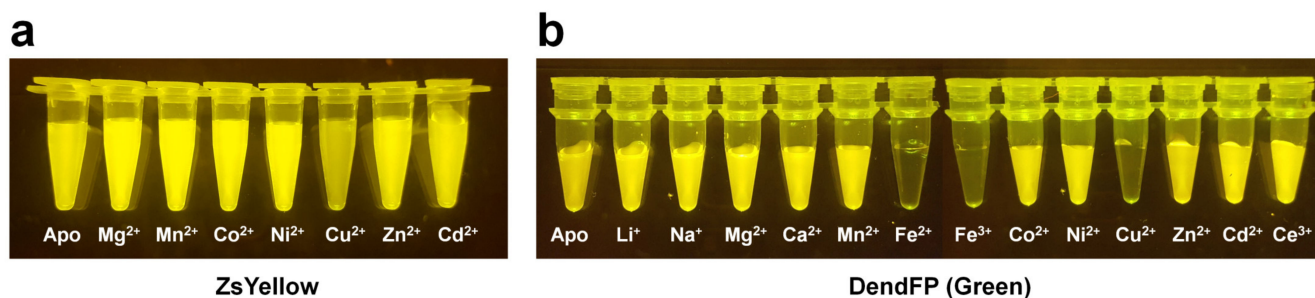


Figure 2. Visualization of quenchable metal ion screening for fluorescent proteins. Fluorescence quenching of (a) ZsYellow and (b) DendFP by metal ions. Original figures were obtained from previous studies for ZsYellow [92] and DendFP [93].

The fluorescence quenching of FPs mediated by metal ions can be caused by static quenching [94], energy transfer between chromophores and quenchable metal ions [95], or perturbations in the FP structure [96]. To develop FP-based metal biosensors, it is important to understand the previous spectroscopic results for the fluorescence quenching of FP mediated by metal ions and the metal binding mechanism on FP. In this review, the spectroscopic characteristics of FP quenching by metals and the quenching mechanism of FP related to metal binding are discussed. In addition, the technologies and prospects required for the future development of FP-based metal biosensors are discussed.

2. Spectroscopic Properties of Metal-Induced FP

Metal-induced fluorescence quenching of various FPs has been spectroscopically analyzed. Among them, BFPms1 and iq-mEmerald [9] were protein-engineered to create metal biosensors, whereas DsRed, Dronpa, AmCyan, ZsGreen, ZsYellow, and DendFP were subjected to spectroscopic analysis using recombinant proteins without protein engineering. The spectroscopic, biochemical, and structural analyses of the FP using metal ions are summarized in Table 4.

These characterized FPs showed unique metal ion selectivity, affinity, and reversibility, as well as different fluorescence quenching intensities, depending on the type of metal ion. Among these characterized FPs, the quenchable metal binding site of DsRed, mBFP1, Iq-mEmerald, and Dronpa have been identified through chemical modification or the X-ray crystallographic method (Table 5).

Table 4. Summary of characterized metal-induced fluorescence-quenched fluorescent proteins.

FP	λ_{ex}	λ_{em}	Chromophore Sequence	Quenchable Metal Ion	K_d (μ M)	Reference
DsRed	558	583	QYG	Cu^{2+}	14.80	[97]
mBFP1	374	447	THG	Cu^{2+}	24	[35]
Iq-mEmerald	450	509	TYG	Cu^{2+}	0.2	[9]
Dronpa ¹	448	518	CYG	Cu^{2+}	N/A	[98]
AmCyan	474	486	MYG	Cu^{2+}	56.10	[99]
mOrange2	549	565	TYG	Cu^{2+}	21.46	[99]
ZsYellow ¹	529	539	KYG	Cu^{2+}	N/A	[92]
ZsGreen	496	506	NYG	Fe^{2+}	11.5	[100]
				Fe^{3+}	16.3	
				Cu^{2+}	68.2	
DendFP (green)	492	508	HYG	Fe^{2+}	24.59	[93]
				Fe^{3+}	41.66	
				Cu^{2+}	137.18	

¹ Dissociation constant was not measured.

Table 5. Metal-binding site of metal-induced fluorescence quenchable fluorescent proteins.

FP	PDB Code	Resolution (\AA)	Metal Ion	Interaction Residues	Reference
DsRed ¹			Cu^{2+}	Cys117	[97]
mBFP1 ²	1KYR	1.50	Cu^{2+}	Chromophore	[35]
	1KYS	1.44	Zn^{2+}	Chromophore	
Iq-mEmerald ²	4KW8	2.46	Ni^{2+}	H202-H204	[9]
	4KW9	1.80	Zn^{2+}	H202-H204	
Dronpa ²	5HZS	2.17	Co^{2+}	H202-H212	[98]
	5HZZ	2.84	Cu^{2+}	H194-H202	
	5HZU	1.89	Ni^{2+}	H202-H212	

¹ Metal ion-binding sites were identified using chemical modification experiments. ² Metal ion-binding sites were identified using X-ray crystallographic experiments.

This review specifically addresses the spectroscopic and structural characterizations of metal-fluorescence-quenched FPs reported to date. Although some experiments on metal-induced fluorescence quenching for EBFP2, mCerulean3, mEmerald, mVenus, mApple, and mKate2 have also been reported [9], they have not been discussed in detail; therefore, they are omitted from this review.

2.1. DsRed

DsRed (DrFP583) is a red fluorescent protein cloned from reef corals [101]. Eli and Chakrabartty investigated the fluorescent emission changes in response to metal ions in DsRed and its mutant proteins (gRF, Rmu74, Rmu80, Rmu162, and Rmu13) [97]. DsRed, Rmu13, and gRF showed a high percentage of quenching of Cu^{2+} , whereas the mutants Rmu74, Rmu80, and Rmu162 showed modest quenching of Cu^{2+} , indicating that the quenching effect of the metal can differ among the mutants despite using red fluorescence of the same origin. Rmu13 was characterized by dual-fluorescence emission peaks at 500 and 580 nm. The titration of DsRed (blue- and red-shifted mutants) and Rmu13 with Cu^{2+} yielded binding constants of 15 and 11 mM, respectively. Moreover, Sumner et al. reported that copper in the binding constant of DsRed is 0.5 mM [102], which differs from

that reported by Eli and Chakrabartty. This apparent discrepancy is due to differences in the formulas for calculating the binding constants, which indicates the need for formalization of the binding constant calculation method applied when developing FP-based metal biosensors (see Section 3 Discussion). The dissociation constant (K_d) of the copper-binding site of DsRed and Rmu13 was approximately 14.80 and 10.90 μM , respectively.

Although structural evidence for quenchable metal binding to DsRed has not been reported yet, biochemical and spectral analyses clearly show a Cu^{2+} -binding site on DsRed. Eli and Chakrabartty investigated copper binding after chemical modification using iodoacetamide and diethyl pyrocarbonate (DEPC) of cysteine and histidine residues, respectively, to trace the Cu^{2+} -binding site of DsRed [97]. As a result, K_d increased by $>100 \mu\text{M}$ when treated with iodoacetamide, whereas no remarkable difference was observed upon treatment with DEPC [97]. This result indicates that the cysteine residue of DsRed is involved in Cu^{2+} -binding [97]. Rahimi et al. investigated the mechanism of DsRed fluorescence quenching: far-UV CD spectral analysis showed no structural changes in the entire protein, even when DsRed was bound to a metal ion [103]. In addition, the UV-visible spectra and Stern–Volmer constant showed a static quenching mechanism during the interaction between DsRed and Cu^{2+} [103]. The crystal structure of DsRed showed a tetramer with 222 non-crystallographic symmetry [104] (Figure 3a).

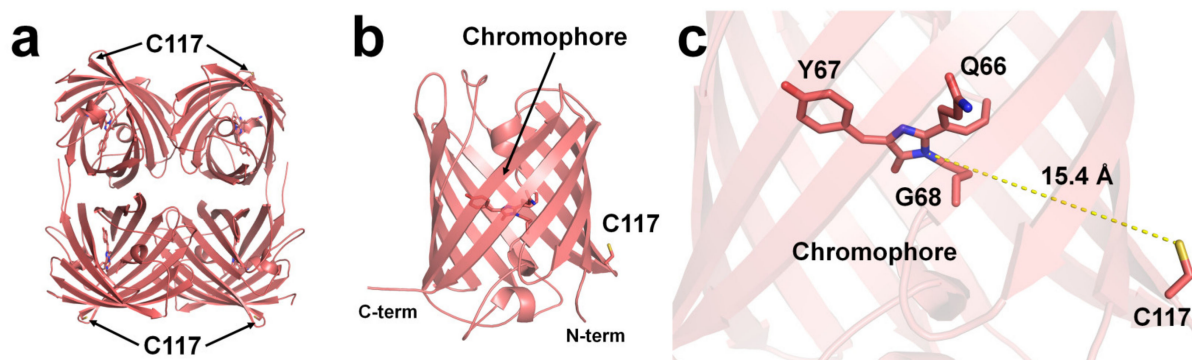


Figure 3. The Cu^{2+} -binding site of DsRed (PDB code 1GGX). The position of Cu^{2+} -binding Cys117 residue on the surface of β -can of (a) tetrameric and (b) monomeric DsRed. The Cu^{2+} -binding site is identified based on chemical modification and spectral analysis. (c) The average distance between the imidazolinone ring of the chromophore and Cys117 in DsRed was 15.4 \AA .

To understand the Cu^{2+} -binding site of DsRed, the deposited crystal structure of DsRed (PDB code 1GGX) was analyzed. The Cys117 residue, which can bind Cu^{2+} of DsRed, was located on the β 7-strand of the β -can surface (Figure 3a,b). The closest distance between the sulfhydryl of Cys117 and the imidazolinone ring of the chromophore was approximately 15.4 \AA (Figure 3c). Because the DsRed monomer contains only one cysteine residue, the tetrameric DsRed can bind four Cu^{2+} ions (Figure 3a). Moreover, as Cys117 of DsRed was located on the surface of β -can, the chelator can easily remove the Cu^{2+} bound to Cys117, which is consistent with the previous spectral results [97].

2.2. BFPms1

BFPms1 is an engineered fluorescent protein that uses a specific metal to bind GFP and alter its fluorescence signal [35]. To create the chromophore of BFPms1 as a metal ligand, such as porphyrin, Tyr66 (corresponding to the chromophore) was substituted with a histidine residue. In particular, Barondeau et al. have developed an H148G mutant to generate holes between β -strands for metal access (Figure 4a). Moreover, additional amino acid substitutions were performed to increase quantum yield (Y145F), improve solubility (F64L, F99S, M153T, and V163A), and promote rapid chromophore formation (S65T). The metal ion screening results showed that Cu^{2+} quenched the fluorescence emission whereas Zn^{2+} enhanced it. BFPms1 has a K_d of 24 μM and 50 μM for Cu^{2+} and Zn^{2+} , re-

spectively, whereas K_D is greater than 2 mM for other transition metal ions [35]. The crystal structures of BFPms1 complexed with Zn^{2+} and Cu^{2+} were determined at a resolution of 1.44 and 1.50 Å, respectively. In Zn-bound BFPms1 (PDB code 1KYS), Zn^{2+} exhibited a trigonal bipyramidal geometry distorted by the chromophore Glu222 and water molecules (Figure 3b). In Cu-bound BFPms1 (1KYR), a square-planar geometry was exhibited by the amino acid Glu222 and the porphyrin of the chromophore (Figure 3c). The histidine ring of BFPms1 exhibited a metal bond shift and rearrangement of Glu222. Structural changes around the chromophore have been shown to occur depending on the type of metal ion bonded to the chromophore. However, it has not been clarified whether the fluorescence emission is changed by the conformational change of the chromophore or whether a metal is bound to the chromophore and has an effect. In this review, additional metal ions binding to the surface of β -can from coordinates deposited in PDB (PDB code 1KYR and 1KYS) were observed. In the BFPms1- Zn^{2+} structure, three additional Zn^{2+} ions interacted with the His25, Glu142, and Glu172 residues, whereas in BFPms1- Cu^{2+} , Mg^{2+} ions interacted with Glu142 in the final model structure. In a structural study of BFPms1, only the metal around the chromophore was described [35], and further studies are required to determine whether the metal bound to the surface of BFPms1 affects fluorescence emission.

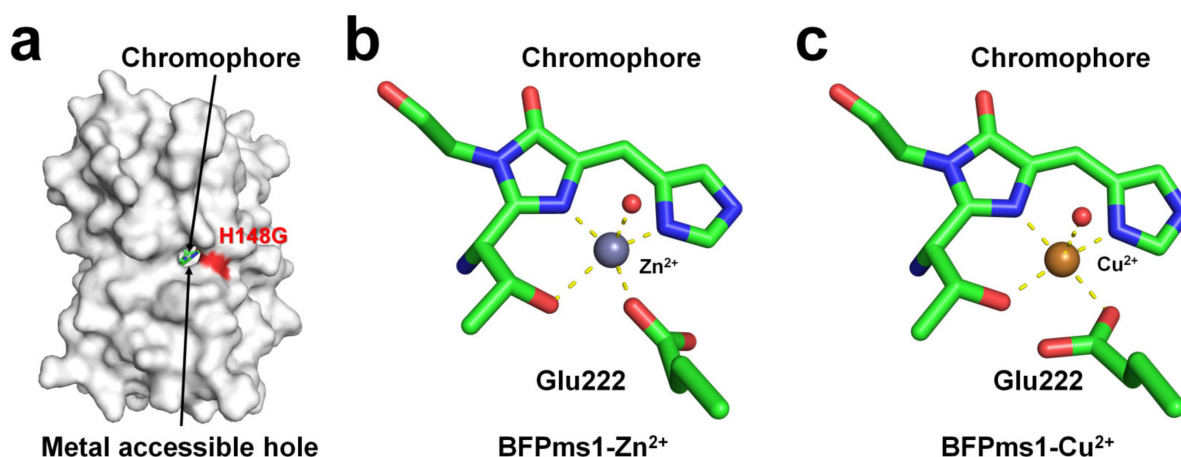


Figure 4. Crystal structure of native, Zn-bound (PDB code 1KYS), and Cu-bound (PDB code 1KYR) state of BFPms1. (a) Surface structure of BFPms1 showed an engineered hole, where the metal ion is accessible. (b) Zn^{2+} and (c) Cu^{2+} binding to the chromophore of BFPms1.

2.3. *iq-mEmerald*

Two surface-exposed histidine residues separated by one residue of the β -sheet (i and $i+2$) create robust transition metal ion binding sites in proteins [95,105]. Using this protein engineering concept, Yu et al. have generated mutant constructs of mEmerald-1H (His147), mEmerald-2H (His202 and His204), and mEmerald-3H (His147, His202, and His204). In mEmerald-2H, two histidine residues are located on the same β 10-strand [9]. In Emerald-3H, the His147 residue is located at the β 7-strand, which is the closest neighbor position of the two histidine residues of mEmerald-2H. mEmerald-2H and mEmerald-3H showed strong fluorescent quenching for Cu^{2+} with a K_d of 0.3 and 0.2 μ M, respectively, whereas wild-type mEmerald and mEmerald-1H showed weak (at high concentration) or low affinity (1–10 μ M), respectively. Accordingly, Yu et al. have generated the most robust and sensitive mEmerald-3H mutant (*iq-mEmerald*) for Cu^{2+} -induced fluorescence quenching. Physiological concentrations of Ca^{2+} (1 mM) and Mg^{2+} (10 mM) did not affect the fluorescence quenching behavior of *iq-mEmerald*. The engineered histidine motif of *iq-mEmerald* can bind specifically to other transition metal ions, such as Co^{2+} , Ni^{2+} , and Zn^{2+} . The crystal structure of *iq-mEmerald* complexed with Ni^{2+} (PDB code 4KW8) and Zn^{2+} (4KW9) ions were determined at a resolution of 2.45 Å, and 1.80 Å, respectively (Figure 5a). Both Ni^{2+} and Zn^{2+} interacted with His202 and His204 of *iq-mEmerald*; however, the con-

formations of the side chains of the metal-interacting histidine residues differed (Figure 5b). In native iq-mEmerald, the side chains of His202 and His204 were in the direction opposite to the metal-binding site. In iq-mEmerald-Ni²⁺, the side chains of His202 and His204 were rotated toward the metal-binding site, and Ni²⁺ was coordinated by His202 and His204 at a distance of 2.08 and 2.04 Å, respectively. In contrast, in iq-mEmerald-Zn²⁺, the conformation of His202 was similar to the conformation of His202 in metal-free iq-mEmerald, whereas the side chain of His204 was rotated to Zn²⁺ ion. Zn²⁺ was coordinated by His202 and His204 at a distance of 2.01 and 2.00 Å, respectively. The closest distance between the imidazoline ring and metal-binding site for Ni²⁺ and Zn²⁺ was approximately 15.7 and 13.4 Å, respectively (Figure 5c). This result indicates that the metal-binding configuration and the distance between the metal ion and chromophore differ depending on the type of metal ion, although the metal-binding sites are the same.

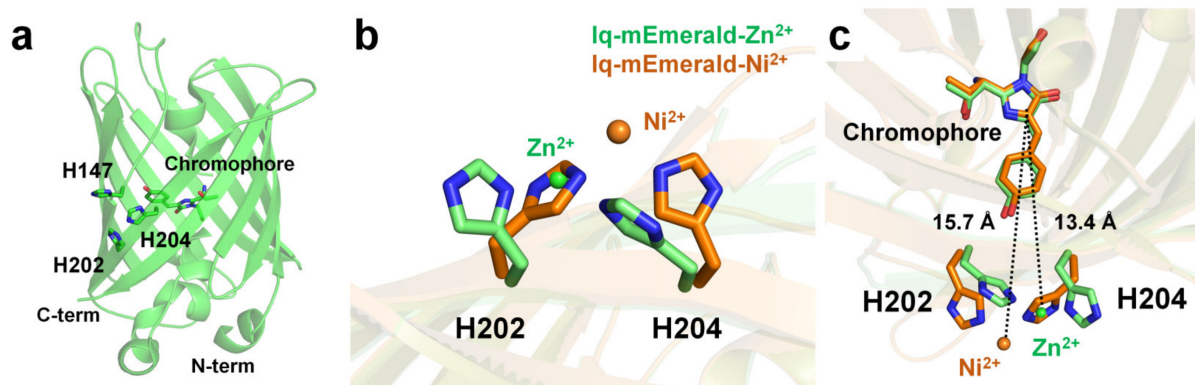


Figure 5. Crystal structure of the native and metal-bound states of iq-mEmerald. (a) Engineered sites (H147, H202 and H204) of iq-mEmerald for metal binding. (b,c) Comparison of the metal-binding site between apo (green) and nickel-bound (orange) structures.

In contrast, in iq-mEmerald-Zn²⁺ (PDB code 4KW8) deposited in PDB, one Cl[−] was modeled at a position 2.24 Å away from Zn²⁺ interacting with His202 and H204. Moreover, in the final model structure of iq-mEmerald-Zn²⁺, four Zn²⁺ were observed, which interacted with Glu124, His139, His147, and His169. However, the effect of the addition of metal ions has not yet been described in related structural studies [9]. Accordingly, it is necessary to investigate the metal-binding sites observed at nonengineered locations and further study their effects on fluorescence emission. This structural information is useful for understanding the metal-binding moiety for further engineering of FP-based metal biosensors. In addition, because the crystal structure of iq-mEmerald complexed with the most effective quencher Cu²⁺ has not yet been determined, further crystallographic studies of Cu²⁺-bound iq-mEmerald are required to better understand the molecular mechanism of Cu²⁺ binding to iq-mEmerald.

2.4. Dronpa

Dronpa is a photoswitchable green fluorescent protein isolated from the *Echinophyllia* sp. SC22 [85]. The Dronpa chromophore consists of a CYG tripeptide with maximum excitation and emission wavelengths of 503 and 518 nm, respectively [85]. The cysteine residue of the Dronpa chromophore is critical for its photoswitchable function [106]. The optical properties of metal-induced fluorescence quenching of Dronpa were screened using divalent ions such as Mg²⁺, Ca²⁺, Mn²⁺, Co²⁺, Ni²⁺, Cu²⁺, Zn²⁺, or Co²⁺ [98]. Cu²⁺ clearly exerted the strongest quenching effect on the fluorescence emission of Dronpa, and Co²⁺ reduced the fluorescence intensity, whereas other metal ions did not significantly affect the fluorescence intensity of Dronpa. The fluorescence intensity of Dronpa quenched by Cu²⁺ and Co²⁺ was reversible and recovered by 97% and 95%, respectively, upon the addition of an EDTA chelator. Dronpa naturally has three histidine residues (His194, His210, and His212) located on the surface of the β-barrel. The crystal structures of Dronpa complexed

with Co^{2+} , Ni^{2+} , and Cu^{2+} had a resolution of 2.20, 1.90, and 2.85 Å, respectively. In the Dronpa- Co^{2+} , the Co^{2+} interacted with the His194 and His212 residues at a distance of 2.21 and 2.26 Å, respectively, and showed distorted octahedral coordination along with four water molecules. In Dronpa- Ni^{2+} , the Ni^{2+} interacted with the His194 and His212 residues at 2.12 and 2.19 Å, respectively, and showed distorted octahedral coordination along with four water molecules. Accordingly, the metal coordination features of Dronpa- Co^{2+} and Dronpa- Ni^{2+} were similar but distinct from those of the surrounding water molecules. The distance between $\text{Co}^{2+}/\text{Ni}^{2+}$ and the imidazoline ring of the chromophore was approximately 14.4 Å. In Dronpa- Cu^{2+} , Cu^{2+} metal interacts with His210 and His212 at distances of 2.34 and 2.54 Å, respectively. However, the Cu^{2+} -binding coordination was not clear because of the poor electron density map. The side chains of His210 and His212 were rotated to the Cu^{2+} -binding site by 90° and 115° , respectively, compared with the native Dronpa structure. Accordingly, when Dronpa interacts with a metal, the histidine residue at the binding site undergoes a conformational rearrangement, indicating that the metal has a geometrically stable configuration. The distance between Cu^{2+} and the imidazoline ring of the chromophore is approximately 14.9 Å. In this study, the metals around the chromophore were described [98]; however, additional metal ions were present at the bottom of the β -barrel in the deposited crystal structure. In Dronpa- Co^{2+} , - Cu^{2+} , and - Zn^{2+} , additional metal ions were bound to His200, and the side chain was exposed to the solvent (Figure 6a). Moreover, the distance between the imidazoline ring of the chromophore and His200 was approximately 19 Å. Accordingly, further experiments are required to determine whether the metal bound to His200 affects the fluorescence-quenching ability of Dronpa.

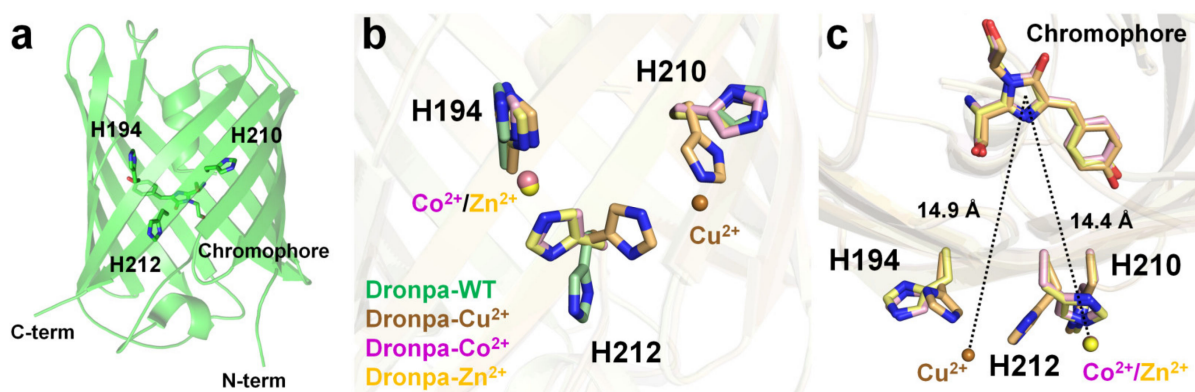


Figure 6. Crystal structure of native (PDB code 2GX2) and the Cu^{2+} - (5HZT), Co^{2+} - (5HZS), and Zn^{2+} - (5HZU)-bound-state of Dronpa. (a) Dronpa contains three native histidine residues (H194, H210, and H212) on the β -can as the metal-binding site. (b) Comparison of the metal-binding site and the conformational change of histidine residues in Dronpa. (c) Measurement of distance between the metal ion and the chromophore of Dronpa.

2.5. AmCyan

AmCyan is a cyan fluorescent protein derived from *Anemonia majano* with two amino acid substitutions (N34S and K68M) that enhance its fluorescence emission [107]. The AmCyan chromophore consists of an MYG tripeptide with maximum absorption and emission wavelengths of 458 and 489 nm, respectively. Quenchable metal ions against AmCyan were screened with mono- or divalent metal ions such as Li^+ , Na^+ , K^+ , Mg^{2+} , Ca^{2+} , Mn^{2+} , Co^{2+} , Ni^{2+} , Cu^{2+} , and Zn^{2+} [99]. AmCyan exhibited 80% fluorescence quenching by Cu^{2+} , followed by 50% and 40% fluorescence quenching by Co^{2+} and Zn^{2+} , respectively [99]. Time-resolved fluorescence monitoring showed that the fluorescence of AmCyan gradually decreased until approximately 7 min; however, the fluorescence intensity slightly increased after 7 min. This result indicates that some Cu^{2+} ions were not tightly bound to AmCyan. In addition, Cu^{2+} titration showed that the K_d and maximum binding capacity (B_{\max}) of AmCyan was 56.10 μM and 102, respectively, according to the Langmuir equation.

Reversibility experiments showed that Cu^{2+} -induced fluorescence-quenched AmCyan was recovered by the EDTA chelator and that the fluorescence intensity of AmCyan was increased by approximately 40% compared to that of the wild-type AmCyan. This finding indicates that AmCyan has a high reversibility for Cu^{2+} and can be used multiple times in various applications. Analysis of the amino acid and modeling structure showed that the His218 residue of AmCyan was positionally identical to the Cu^{2+} -binding residue His212 of Dronpa [99].

2.6. *mOrange2*

The fluorescent protein *mOrange2* is an orange fluorescent protein derived from DsRed [72], and *mOrange2* was engineered from *mOrange* with four amino acid substitutions (Q64H, F99Y, E160K, and G196D). The chromophore of *mOrange2* consists of a TYG tripeptide with maximum excitation and emission wavelengths of 549 and 565 nm, respectively. Quenchable metal ions against *mOrange2* were screened with mono- or divalent metal ions such as Li^+ , Na^+ , K^+ , Mg^{2+} , Ca^{2+} , Mn^{2+} , Co^{2+} , Ni^{2+} , Cu^{2+} , and Zn^{2+} [99]. The highest fluorescence quenching of *mOrange2* was observed for Cu^{2+} , which reduced the fluorescence emission by 89% [99]. Other divalent metal ions, such as Co^{2+} , Zn^{2+} , and Ni^{2+} reduce the fluorescence emission by less than 7%, whereas other monovalent metal ions have no effect. These spectroscopic results indicate that *mOrange2* is highly selective and sensitive to Cu^{2+} . Moreover, time-resolved fluorescence quenching monitoring of *mOrange2* using Cu^{2+} for 20 min showed that the fluorescence intensity continuously decreased, indicating that the binding of Cu^{2+} to *mOrange2* was irreversible. The Cu^{2+} -titration of *mOrange2* result showed K_d and B_{\max} of 21.46 μM and 86, respectively, using the Langmuir equation. Reversibility experiments using EDTA chelators showed that the fluorescence intensity of quenched *mOrange2* by Cu^{2+} was completely recovered, indicating that *mOrange2* has a high reversibility for Cu^{2+} and can be used multiple times in terms of applications. The modeled structure of *mOrange2* was generated and compared with previously reported metal-binding FPs, showing that *mOrange2* has a unique metal-binding site that may differ from the metal-binding site of *iq-mEmerald* and Dronpa.

2.7. *ZsYellow*

ZsYellow is a green fluorescent protein derived from zFP538 of *Zoanthus* sp. [56]. The *ZsYellow* chromophore consists of a KYG tripeptide, which constitutes a three-ring system formed by the heterocyclization of Lys66 [56]. As a result, the backbone between Phe65 and Lys66 was cleaved, consistent with previous reports on zFP538 [108]. The excitation and emission wavelengths of *ZsYellow* were 527 and 540 nm, respectively. Metal-induced fluorescence quenching of *ZsYellow* was screened using divalent metal ions such as Mg^{2+} , Mn^{2+} , Co^{2+} , Ni^{2+} , Cu^{2+} , Zn^{2+} , or Cd^{2+} [92]. Cu^{2+} highly quenched the fluorescence emission of *ZsYellow* by 81.4%, and Co^{2+} , Ni^{2+} , and Cd^{2+} also reduced the fluorescence emission of *ZsYellow* by 54.0, 35.2, and 32.1%, respectively. Li^+ , Na^+ , Ca^{2+} , Mn^{2+} , Zn^{2+} , and Ce^{2+} caused modest reductions in *ZsYellow* fluorescence intensity of 11.22, 7.49, 14.32, 21.1, 25.9, and 3.51%, respectively. The results indicated that the fluorescence of *ZsYellow* showed the highest sensitivity to Cu^{2+} when compared to the other screened metal ions. To identify the quenchable metal-binding site in *ZsYellow*, a crystallographic study of *ZsYellow* complexed with Cu^{2+} was conducted. When the *ZsYellow* crystals were immersed in a solution containing Cu^{2+} , the crystals were in a transparent state, and the yellow color of the crystals disappeared, indicating that the crystals were in a state of fluorescence quenching (Figure 7a). Interestingly, in the crystal structure of *ZsYellow* soaked with Cu^{2+} , electron density maps corresponding to Cu^{2+} were not observed. However, when comparing native *ZsYellow* and Cu^{2+} -soaked crystals, a small conformational change in the cyclic ring in the chromophore was observed (Figure 7b). A similar conformational change in the cyclic ring of *ZsYellow* was observed in its fluorescence-quenched state at low pH [56]. However, whether this structural change was caused by fluorescence quenching has not yet been clarified. Based on these crystallographic results, *ZsYellow* indicated that Cu^{2+} is capable

of fluorescence quenching in a nonspecific metal-binding manner, owing to the absence of an electron density map corresponding to Cu^{2+} .

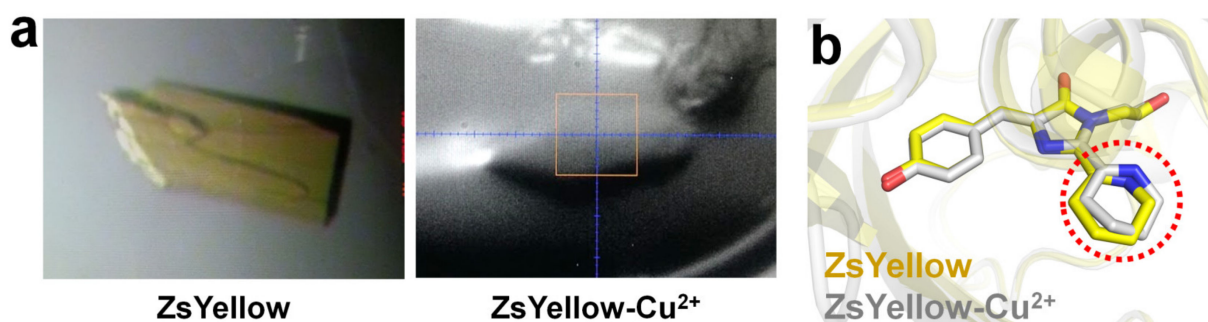


Figure 7. Crystallographic study of ZsYellow. (a) Color change of the ZsYellow crystal by Cu^{2+} solution soaking. (b) Comparison between the chromophore of the native and Cu^{2+} -soaked ZsYellow. Original figures were obtained from a previous study [92] and modified.

2.8. ZsGreen

ZsGreen is an engineered green fluorescent protein derived from GFP506 from *Zoanthus* sp., in which Asn65 is replaced by methionine to improve the fluorescent emission characteristics [101,109]. ZsGreen has a chromophore composed of an MYG tripeptide with excitation and emission maxima at 496 and 506 nm, respectively. The fluorescence quenching of ZsGreen was screened using various metal ions such as Li^+ , Na^+ , Mg^{2+} , Ca^{2+} , Mn^{2+} , Fe^{2+} , Fe^{3+} , Co^{2+} , Ni^{2+} , Cu^{2+} , Zn^{2+} , Cd^{2+} , and Ce^{2+} [100]. Fe^{2+} and Fe^{3+} significantly quenched the fluorescence emission of ZsGreen by 1.1 and 3.5%, respectively, whereas Cu^{2+} quenched the fluorescence emission of ZsGreen by 22.8%. Co^{2+} , Ni^{2+} , Zn^{2+} , and Cd^{2+} showed moderate fluorescence quenching of 77.4, 87.4, 62.7, and 81.0%, respectively, whereas no significant fluorescence changes were observed for the other metal ions. In addition, titration experiments using ZsGreen showed that the K_d values of Fe^{2+} , Fe^{3+} , and Cu^{2+} for ZsGreen were 11.5, 16.3, and 68.2 μM , respectively. The B_{max} values of ZsGreen in the presence of Fe^{2+} , Fe^{3+} , and Cu^{2+} were 103.3, 102.2, and 82.9, respectively. Consequently, ZsGreen was efficiently quenched by Fe ions. Reversibility experiments using EDTA showed that Cu^{2+} -incubated ZsGreen showed 82% recovery, whereas Fe^{2+} - and Fe^{3+} -treated ZsGreen showed 15.9% and 13.3% reversibility, respectively. The high sensitivity of ZsGreen to Fe ions is attractive; however, it has low reversible efficiency for Fe ions, making it less attractive in terms of cost or reusability in terms of applications. Analysis of the amino acid sequence and model structure of ZsGreen showed that the metal-binding site of ZsGreen does not share the previously reported metal-binding sites of iq-mEmeral or Dronpa. This result indicates that ZsGreen has a novel quenched metal-binding site that is distinct from that of previously reported metal-binding fluorescent proteins.

2.9. DendFP

DendFP is a photoconvertible fluorescent protein belonging to the Kaede-like group, derived from the *Dendronophya* sp. [110,111]. The chromophore of DendFP consists of an HYG tripeptide, a protein that irreversibly converts green to red when exposed to the light of a specific wavelength. The excitation/emission peak wavelengths of DendFP in the green and red states are 492/508 and 555/575 nm, respectively [110,111]. The fluorescence quenching of DendFP in the green state by metal ions was investigated [93]. However, the fluorescence spectrum of the recombinant green-state FP used in the experiment showed a main peak at 508 nm and a minor peak at 575 nm. This indicated that some DendFPs were partially converted to the red state during the sample preparation process. Fluorescence quenching of the green state of DendFP was screened using various metal ions, such as Li^+ , Na^+ , Mg^{2+} , Ca^{2+} , Mn^{2+} , Fe^{2+} , Fe^{3+} , Co^{2+} , Ni^{2+} , Cu^{2+} , Zn^{2+} , Cd^{2+} , and Ce^{3+} [93]. Notable fluorescence quenching of DendFP was observed for Fe^{2+} , Fe^{3+} , and Cu^{2+} . Moderate fluorescence reduction of DendFP was also observed for Co^{2+} , Ni^{2+} , Zn^{2+} , and Cd^{2+} in the

range of 12–15%, whereas other metal ions were not critical for fluorescence quenching. Titration experiments showed that K_d of Fe^{2+} , Fe^{3+} , and Cu^{2+} for DendFP were 24.59, 41.66, and 137.18 μM , respectively. The B_{max} of Fe^{2+} , Fe^{3+} , and Cu^{2+} for DendFP were 104.47, 105.28, and 100.46, respectively.

To identify the quenching mechanism, fluorescence quenching of DendFP was measured at two different temperatures (25 °C and 35 °C). Analysis of the titration results based on the Stern–Volmer equation showed that Fe^{2+} and Cu^{2+} reveal a dynamic process during fluorescence quenching; however, the quenching mechanism of DendFP by Fe^{3+} was not identified because there was no difference between the two different temperatures. The reversibility of DendFP activity was investigated using EDTA and EGTA. Cu^{2+} exhibits better reversibility than Fe^{2+} and Fe^{3+} after treatment with EDTA. EGTA is an effective chelator for the reversibility of DendFP quenching by Fe^{2+} and Fe^{3+} , compared to EDTA. Moreover, the reversibility efficiency of FP quenched by Fe^{2+} and Fe^{3+} differed, indicating that the reversibility of DendFP by EDTA or EGTA depends on the transition state of the metal ions. To identify the quenchable metal-binding site of DendFP, crystal soaking experiments with quenchable metal ions were performed; however, the crystals were distorted, and the crystal structure of the metal-bound state of DendFP was not successfully collected. Although the direct metal-binding site of DendFP has not been clarified, this soaking experiment indicates that quenchable metal ions could affect the crystal packing of the surface of DendFP. In addition, analysis of the tetrameric assembly of the crystal structure of DendFP suggested that the interface of the monomer of DendFP in tetrameric assembly is not involved in the quenchable metal-binding site [93], which is consistent with the reversibility experiment reporting quenchable metal ion binding to the solvent-exposed surface of β -can (Figure 8).

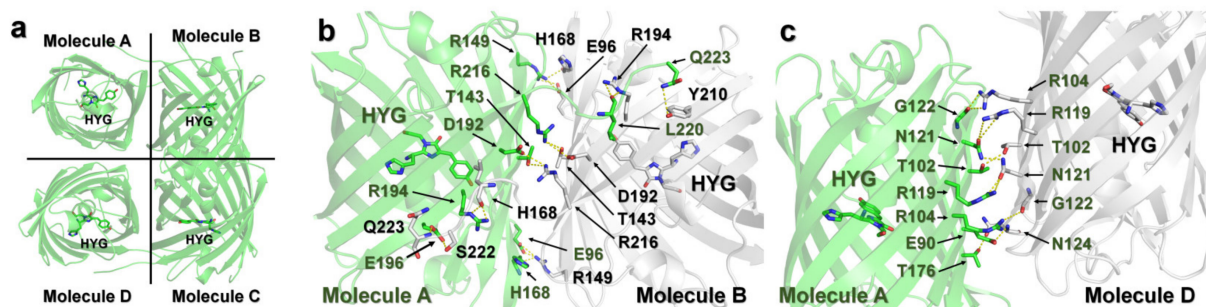


Figure 8. Crystal structure of the green state of DendFP (PDB code 7DIG). (a) DendFP forms the tetrameric formation, indicating that the quenchable metal ion could interact with the surface of the tetrameric assembly of DendFP. (b,c) Interface of the DendFP monomer in the tetrameric assembly showed no space for metal binding and access to metal chelator. Original figures were obtained from a previous study [93].

3. Discussion

FPs are widely used as optical probes in various molecular and cellular biological studies. The fluorescence emission properties of the FP can be altered by external stimuli. In particular, the fluorescence quenching of FP mediated by metal ions is an attractive metal biosensor probe for measuring metal ion levels. In this review, various intrinsic FPs and their applications are introduced and research on eight FPs that performed fluorescence quenching using metal ions are reviewed. The results of individual spectroscopy studies on the aforementioned metal-induced FPs tentatively indicate the potential for applications of FP-based metal biosensors. FPs reported to date show high sensitivity to Cu^{2+} and exhibit fluorescence-quenching characteristics. Several neurodegenerative diseases (Alzheimer’s disease, prion disease, and amyotrophic lateral sclerosis) exhibit the characteristic presence of aggregated protein deposits [97,112,113]. These neurodegenerative diseases share a common feature of deposition mechanism is that the aggregation of each protein is promoted by Cu^{2+} binding [113–115]. FPs with high Cu^{2+} sensitivity can be used

to probe the Cu content in protein aggregates in these neurodegenerative diseases as well as other diseases [97]. Accordingly, they can be used to detect Cu^{2+} levels using a previously reported Cu^{2+} -sensitive FP; however, several additional metal screens must be performed. As reviewed here, DsRed, BFPms1, iq-mEmerald, Dronpa, AmCyan, and ZsYellow showed the highest fluorescence quenching for Cu^{2+} but were not screened for all transition metal ions. In the extended metal-induced fluorescence quenching experiment of ZsGreen and DendFP, both proteins showed remarkable fluorescence quenching by Cu^{2+} but were more sensitive to fluorescence quenching by Fe^{2+} and Fe^{3+} . If Fe^{2+} , Fe^{3+} , or heavy metal ions are treated with DsRed, BFPms1, iq-mEmerald, Dronpa, AmCyan, and ZsYellow, they may exhibit higher fluorescence quenching properties than Cu^{2+} . In fact, it was confirmed that ZsYellow showed greater fluorescence quenching by Fe^{2+} than by Cu^{2+} (unpublished data). Moreover, although ZsGreen and DendFP showed the highest fluorescence quenching properties in the presence of Fe^{2+} and Fe^{3+} , indicating that if screening is performed using more extended metal ions, including heavy atoms, it is possible to identify metal ions that are more effective in fluorescence quenching. Therefore, for previously reported metal ions capable of quenching fluorescence, it cannot be concluded that they show the highest sensitivity for the corresponding FP because only the metal ions selected by the researchers were tested. Accordingly, in the future, in addition to the metal ions commonly encountered in laboratories, screening for various extended metal ions, including heavy metal ions, will be required.

The data of the studies used for fluorescence quenching of the reviewed FPs provided the dissociation constant values of metal ions based on spectroscopic results. However, the metal titration results were not calculated using a unified formula. Accordingly, as in the results for DsRed, different K_d values can be obtained by applying a distinct empirical formula to the same experiment in two laboratories [97]. Moreover, the methods for measuring fluorescence quenching by metals of the FPs reported in this review are different. FP concentration, temperature, buffer, or pH of the measurement solution are factors that can affect fluorescence quenching. Therefore, a direct comparison of spectroscopic results for fluorescence quenching of characterized FPs by metals is not possible. Accordingly, in the process of developing FP-based biosensor probes in the future, it will be necessary to discuss the application of standardized methods and equations related to metal binding in the related community to compare the metal-binding abilities of independent proteins. Future experiments should determine the lowest concentration of an analyte that can be detected and quantified, such as the limit of detection (LOD) and limit of quantification (LOQ), which is an indicator of the performance of the sensor and provides information on whether the actual FP can be applied as a biosensor probe [116,117]. Moreover, among the FPs reviewed in this paper, the various characteristics of DendFP were well spectroscopically analyzed, providing valuable information to help evaluate their application as metal biosensor probes, such as screening for quenchable metal ions through various metal ions, measurement of K_d and B_{max} through titration experiments, verification of fluorescence quenching process using Stern–Volmer equation, measurement of reversibility using metal chelator, measurement of metal ion selectivity, and measurement of LOD and LOQ. These measurements are necessary for the evaluation of the applicability of FPs as metal biosensor probes in the future.

In addition, the prediction of the characteristics of fluorescence quenching by metal ions based on the spectroscopic characteristics, amino acid sequence, or structure of fluorescent proteins is impossible. As shown by the fluorescence quenching characteristics of DsRed and its mutants, despite using the same origin, fluorescence quenching characteristics may differ significantly depending on the mutant type [97]. Among the characterized FPs, mOrange2 showed a highly sensitive quenching effect on the specific Cu^{2+} , whereas other metal ions did not affect fluorescence emission [99]. Most other FPs showed fluorescence quenching in the presence of several metal ions. For example, although Dronpa exhibits high fluorescence quenching by Cu^{2+} , notable fluorescence quenching by Co^{2+} has also been observed [98]. Notably, in the crystal structure of Dronpa complexed with metal

ions, Cu^{2+} interacts with H202 and H212 on the β -can surface of Dronpa whereas Co^{2+} interacts with H194 and H212, indicating that different binding sites exist for different types of quenchable metal ions. If Dronpa is reacted with a divalent metal solution containing Cu^{2+} and Co^{2+} , Cu^{2+} and Co^{2+} can bind to the histidine residue on the β -can surface of Dronpa. Although Cu^{2+} will bind more to Dronpa and react more sensitively depending on the binding affinity, it is not possible to determine the amount of Co^{2+} that binds to Dronpa and how much it influences the overall fluorescence quenching. Therefore, Dronpa cannot be used as a biosensor to quantitatively measure Cu^{2+} levels. However, because Cu^{2+} and Co^{2+} have different binding sites for Dronpa, substituting His194 with another amino acid in the histidine residue, to which Co^{2+} binds, removes the preferred binding site for Co^{2+} . This structure-based engineering can generate Dronpa which is capable of fluorescence quenching specifically for Cu^{2+} only. To prevent unwanted metal ion binding to FP, it is possible to engineer unwanted metal-binding sites, which will lead to the development of a more efficient FP-based biosensor. Accordingly, it is important to not only spectroscopically determine the quenchable metal ion for FP but also identify the metal-binding site via structural biology. In addition, this review confirms that additional metal ions interact with histidine or glutamate residues on the β -can surface in the deposited final coordinates for crystal structures of DsRed, BFPms1, and Dronpa complexed with metal ions. Further studies are required to determine whether these additional metal ions, which are involved in the fluorescence quenching effect, are essential. Metal ion binding at these nonspecific positions can cause problems in quantifying metal ion levels for practical applications. Therefore, an engineering method is required to ensure the binding of the desired metal ion only at desired positions.

On the other hand, as mentioned in this review, several FPs exhibit fluorescence quenching by specific transition metal ions without protein engineering. While these fluorescent proteins are intriguing as metal biosensors, their application in quantifying fluorescence levels in molecular or cell biology experiments may pose challenges because the intensity of fluorescence emission can be affected by specific metal ions. Therefore, the characterization of fluorescence quenching of FPs by metal ions can provide useful information for the development of metal biosensors as well as important experimental information for their application as general fluorescent probes. Moreover, continuous investigation of changes in fluorescence emission of FP by specific metals provides important information for assessing the effect on the sample environment related to metal ions across all experimental fields that use FPs as optical probes, including biosensor probe discovery. Although several studies on the fluorescence quenching properties of FPs by metal ions have been summarized in this review, they are still at the stage of performing spectroscopic or structural biological analyses at the molecular level. As presented in Tables 2 and 3, various FPs with intrinsic spectroscopic properties exist in nature or by protein engineering and have various applications; however, the spectroscopic properties of most FPs for fluorescence quenching by metal ions have not yet been reported. Therefore, many libraries have the potential to exhibit superior characteristics as biosensors compared to previously developed metal-sensitive FPs. To develop a FP for use as a metal biosensor, it is necessary to continuously identify new FPs and determine their spectroscopic characteristics along with engineering previously reported metal-sensitive FPs. In particular, when FPs are used as biosensor probes, factors such as high sensitivity and selectivity, low detection limit, fast response, operational simplicity, real-time monitoring, and low cost should be considered. Therefore, when selecting an FP probe in the early developmental stage, it is important to consider the expression level, QY, and brightness of the FP.

Funding: This work was funded by the National Research Foundation of Korea (NRF) (NRF-2017M3A9F6029736 and NRF-2021R1I1A1A01050838) and Korea Initiative for Fostering University of Research and Innovation (KIURI) Program of the NRF (NRF-2020M3H1A1075314). This study was supported by ProGen.

Institutional Review Board Statement: Not applicable.

Informed Consent Statement: Not applicable.

Data Availability Statement: Not applicable.

Conflicts of Interest: The authors declare no conflict of interest.

References

1. Carter, K.P.; Young, A.M.; Palmer, A.E. Fluorescent Sensors for Measuring Metal Ions in Living Systems. *Chem. Rev.* **2014**, *114*, 4564–4601. [[CrossRef](#)] [[PubMed](#)]
2. Moustakas, M. The Role of Metal Ions in Biology, Biochemistry and Medicine. *Materials* **2021**, *14*, 549. [[CrossRef](#)] [[PubMed](#)]
3. Prasad, A.S. Zinc deficiency. *BMJ* **2003**, *326*, 409–410. [[CrossRef](#)] [[PubMed](#)]
4. Theil, E.C. Iron Homeostasis and Nutritional Iron Deficiency. *J. Nutr.* **2011**, *141*, 724S–728S. [[CrossRef](#)]
5. Tang, Z.; Wang, H.Q.; Chen, J.; Chang, J.D.; Zhao, F.J. Molecular mechanisms underlying the toxicity and detoxification of trace metals and metalloids in plants. *J. Integr. Plant Biol.* **2023**, *65*, 570–593. [[CrossRef](#)]
6. Avila, D.S.; Puntel, R.L.; Aschner, M. Manganese in Health and Disease. In *Interrelations between Essential Metal Ions and Human Diseases; Metal Ions in Life Sciences*; Springer: Berlin/Heidelberg, Germany, 2013; pp. 199–227.
7. Zheng, X.; Cheng, W.; Ji, C.; Zhang, J.; Yin, M. Detection of metal ions in biological systems: A review. *Rev. Anal. Chem.* **2020**, *39*, 231–246. [[CrossRef](#)]
8. Mitra, S.; Chakraborty, A.J.; Tareq, A.M.; Emran, T.B.; Nainu, F.; Khuro, A.; Idris, A.M.; Khandaker, M.U.; Osman, H.; Alhumaydhi, F.A.; et al. Impact of heavy metals on the environment and human health: Novel therapeutic insights to counter the toxicity. *J. King Saud Univ. Sci.* **2022**, *34*, 101865. [[CrossRef](#)]
9. Yu, X.; Strub, M.P.; Barnard, T.J.; Noinaj, N.; Piszczek, G.; Buchanan, S.K.; Taraska, J.W. An engineered palette of metal ion quenchable fluorescent proteins. *PLoS ONE* **2014**, *9*, e95808. [[CrossRef](#)]
10. Ghaedi, M.; Ahmadi, F.; Shokrollahi, A. Simultaneous preconcentration and determination of copper, nickel, cobalt and lead ions content by flame atomic absorption spectrometry. *J. Hazard. Mater.* **2007**, *142*, 272–278. [[CrossRef](#)]
11. Ashenef, A. Essential and toxic metals in tea (*Camellia sinensis*) imported and produced in Ethiopia. *Food Addit. Contam. B Surveill.* **2013**, *7*, 30–36. [[CrossRef](#)]
12. Williams, M.; Luo, W.; McWhirter, K.; Ikegbu, O.; Talbot, P. Chemical Elements, Flavor Chemicals, and Nicotine in Unused and Used Electronic Cigarettes Aged 5–10 Years and Effects of pH. *Int. J. Environ. Health Res.* **2022**, *19*, 16931. [[CrossRef](#)]
13. Amerikanou, C.; Karavoltos, S.; Gioxari, A.; Tagkouli, D.; Sakellari, A.; Papada, E.; Kalogeropoulos, N.; Forbes, A.; Kaliora, A.C. Clinical and inflammatory biomarkers of inflammatory bowel diseases are linked to plasma trace elements and toxic metals; new insights into an old concept. *Front. Nutr.* **2022**, *9*, 997356. [[CrossRef](#)]
14. Kim, H.H.; Lee, G.H.; Pyo, G.J.; Kwon, E.S.; Myung, K.B.; Cheong, S.H. Nickel, cobalt, and chromium in nail sticker and tip products in Korea. *Contact Derm.* **2023**. ahead of print. [[CrossRef](#)]
15. Nazir, N.U.A.; Abbas, S.R. Identification of phenol 2,2-methylene bis, 6 [1,1-D] as breath biomarker of hepatocellular carcinoma (HCC) patients and its electrochemical sensing: E-nose biosensor for HCC. *Anal. Chim. Acta* **2023**, *1242*, 340752. [[CrossRef](#)]
16. Patel, M.; Bisht, N.; Prabhakar, P.; Sen, R.K.; Kumar, P.; Dwivedi, N.; Ashiq, M.; Mondal, D.P.; Srivastava, A.K.; Dhand, C. Ternary nanocomposite-based smart sensor: Reduced graphene oxide/polydopamine/alanine nanocomposite for simultaneous electrochemical detection of Cd²⁺, Pb²⁺, Fe²⁺, and Cu²⁺ ions. *Environ. Res.* **2023**, *221*, 115317. [[CrossRef](#)]
17. Loa, J.D.A.; Cruz-Rodríguez, I.A.; Rojas-Avelizapa, N.G. Colorimetric Detection of Metals Using CdS-NPs Synthesized by an Organic Extract of *Aspergillus niger*. *Appl. Biochem. Biotechnol.* **2023**. ahead of print. [[CrossRef](#)]
18. Wang, X.; Liu, S.; Zhou, J.; Zhang, S.; Hou, C.; Huo, D. Colorimetric detection of Cu²⁺ based on the inhibition strategy for etching reaction of AgNCs. *Spectrochim. Acta A Mol. Biomol. Spectrosc.* **2023**, *289*, 122229. [[CrossRef](#)]
19. Lü, B.; Chen, Y.; Li, P.; Wang, B.; Müllen, K.; Yin, M. Stable radical anions generated from a porous perylene diimide metal-organic framework for boosting near-infrared photothermal conversion. *Nat. Commun.* **2019**, *10*, 767. [[CrossRef](#)]
20. Forzani, E.S.; Zhang, H.; Chen, W.; Tao, N. Detection of Heavy Metal Ions in Drinking Water Using a High-Resolution Differential Surface Plasmon Resonance Sensor. *Environ. Sci. Technol.* **2004**, *39*, 1257–1262. [[CrossRef](#)]
21. Malitesta, C.; Guascito, M.R. Heavy metal determination by biosensors based on enzyme immobilised by electropolymerisation. *Biosens. Bioelectron.* **2005**, *20*, 1643–1647. [[CrossRef](#)]
22. Zhu, X.; Xu, L.; Lou, Y.; Yu, H.; Li, X.; Blake, D.A.; Liu, F. Preparation of Specific Monoclonal Antibodies (MAbs) against Heavy Metals: MAbs That Recognize Chelated Cadmium Ions. *J. Agric. Food Chem.* **2007**, *55*, 7648–7653. [[CrossRef](#)] [[PubMed](#)]
23. Lee, J.-S.; Han, M.S.; Mirkin, C.A. Colorimetric Detection of Mercuric Ion (Hg²⁺) in Aqueous Media using DNA-Functionalized Gold Nanoparticles. *Angew. Chem. Int. Ed.* **2007**, *46*, 4093–4096. [[CrossRef](#)] [[PubMed](#)]
24. Li, T.; Shi, L.; Wang, E.; Dong, S. Silver-Ion-Mediated DNAzyme Switch for the Ultrasensitive and Selective Colorimetric Detection of Aqueous Ag⁺ and Cysteine. *Chem. Eur. J.* **2009**, *15*, 3347–3350. [[CrossRef](#)] [[PubMed](#)]
25. Lehmann, M.; Riedel, K.; Adler, K.; Kunze, G. Amperometric measurement of copper ions with a deputy substrate using a novel *Saccharomyces cerevisiae* sensor. *Biosens. Bioelectron.* **2000**, *15*, 211–219. [[CrossRef](#)]
26. Tsien, R.Y. The green fluorescent protein. *Annu. Rev. Biochem.* **1998**, *67*, 509–544. [[CrossRef](#)]
27. Xu, Y.; Hwang, K.Y.; Nam, K.H. Spectral and structural analysis of large Stokes shift fluorescent protein dKeima570. *J. Microbiol.* **2018**, *56*, 822–827. [[CrossRef](#)]

28. Kim, S.E.; Hwang, K.Y.; Nam, K.H. Spectral and structural analysis of a red fluorescent protein from *Acropora digitifera*. *Protein Sci.* **2019**, *28*, 375–381. [[CrossRef](#)]
29. Lee, Y.R.; Park, J.-H.; Hahm, S.-H.; Kang, L.-W.; Chung, J.H.; Nam, K.-H.; Hwang, K.Y.; Kwon, I.C.; Han, Y.S. Development of Bimolecular Fluorescence Complementation Using Dronpa for Visualization of Protein–Protein Interactions in Cells. *Mol. Imaging Biol.* **2010**, *12*, 468–478. [[CrossRef](#)]
30. Bajar, B.T.; Wang, E.S.; Zhang, S.; Lin, M.Z.; Chu, J. A Guide to Fluorescent Protein FRET Pairs. *Sensors* **2016**, *16*, 1488. [[CrossRef](#)]
31. Liao, J.; Madahar, V.; Dang, R.; Jiang, L. Quantitative FRET (qFRET) Technology for the Determination of Protein–Protein Interaction Affinity in Solution. *Molecules* **2021**, *26*, 6339. [[CrossRef](#)]
32. Skruzny, M.; Pohl, E.; Abella, M. FRET Microscopy in Yeast. *Biosensors* **2019**, *9*, 122. [[CrossRef](#)]
33. Baird, G.S.; Zacharias, D.A.; Tsien, R.Y. Circular permutation and receptor insertion within green fluorescent proteins. *Proc. Natl. Acad. Sci. USA* **1999**, *96*, 11241–11246. [[CrossRef](#)]
34. Galletta, L.J.V.; Haggie, P.M.; Verkman, A.S. Green fluorescent protein-based halide indicators with improved chloride and iodide affinities. *FEBS Lett.* **2001**, *499*, 220–224. [[CrossRef](#)]
35. Barondeau, D.P.; Kassmann, C.J.; Tainer, J.A.; Getzoff, E.D. Structural chemistry of a green fluorescent protein Zn biosensor. *J. Am. Chem. Soc.* **2002**, *124*, 3522–3524. [[CrossRef](#)]
36. Bizzarri, R.; Arcangeli, C.; Arosio, D.; Ricci, F.; Faraci, P.; Cardarelli, F.; Beltram, F. Development of a Novel GFP-based Ratiometric Excitation and Emission pH Indicator for Intracellular Studies. *Biophys. J.* **2006**, *90*, 3300–3314. [[CrossRef](#)]
37. Frommer, W.B.; Davidson, M.W.; Campbell, R.E. Genetically encoded biosensors based on engineered fluorescent proteins. *Chem. Soc. Rev.* **2009**, *38*, 2833–2841. [[CrossRef](#)]
38. Tantama, M.; Hung, Y.P.; Yellen, G. Optogenetic reporters. In *Optogenetics: Tools for Controlling and Monitoring Neuronal Activity*; Progress in Brain Research; Elsevier: Amsterdam, The Netherlands, 2012; pp. 235–263.
39. Akerboom, J.; Carreras Calderón, N.; Tian, L.; Wabnig, S.; Prigge, M.; Tolö, J.; Gordus, A.; Orger, M.B.; Severi, K.E.; Macklin, J.J.; et al. Genetically encoded calcium indicators for multi-color neural activity imaging and combination with optogenetics. *Front. Mol. Neurosci.* **2013**, *6*, 2. [[CrossRef](#)]
40. Broyles, C.; Robinson, P.; Daniels, M. Fluorescent, Bioluminescent, and Optogenetic Approaches to Study Excitable Physiology in the Single Cardiomyocyte. *Cells* **2018**, *7*, 51. [[CrossRef](#)]
41. Benaissa, H.; Ounoughi, K.; Aujard, I.; Fischer, E.; Goïame, R.; Nguyen, J.; Tebo, A.G.; Li, C.; Le Saux, T.; Bertolin, G.; et al. Engineering of a fluorescent chemogenetic reporter with tunable color for advanced live-cell imaging. *Nat. Commun.* **2021**, *12*, 6989. [[CrossRef](#)]
42. Miura, Y.; Senoo, A.; Doura, T.; Kiyonaka, S. Chemogenetics of cell surface receptors: Beyond genetic and pharmacological approaches. *RSC Chem. Biol.* **2022**, *3*, 269–287. [[CrossRef](#)]
43. Tanz, S.K.; Castleden, I.; Small, I.D.; Millar, A.H. Fluorescent protein tagging as a tool to define the subcellular distribution of proteins in plants. *Front. Plant Sci.* **2013**, *4*, 214. [[CrossRef](#)] [[PubMed](#)]
44. Cui, Y.; Gao, C.; Zhao, Q.; Jiang, L. Using Fluorescent Protein Fusions to Study Protein Subcellular Localization and Dynamics in Plant Cells. In *High-Resolution Imaging of Cellular Proteins*; Methods in Molecular Biology; Humana Press: New York, NY, USA, 2016; pp. 113–123.
45. Hynes, T.R.; Hughes, T.E.; Berlot, C.H. Cellular Localization of GFP-Tagged α Subunits. In *G Protein Signaling*; Humana Press: New York, NY, USA, 2003; pp. 233–246.
46. Chudakov, D.M.; Lukyanov, S.; Lukyanov, K.A. Fluorescent proteins as a toolkit for in vivo imaging. *Trends Biotechnol.* **2005**, *23*, 605–613. [[CrossRef](#)]
47. Lippincott-Schwartz, J. Emerging In Vivo Analyses of Cell Function Using Fluorescence Imaging. *Annu. Rev. Biochem.* **2011**, *80*, 327–332. [[CrossRef](#)] [[PubMed](#)]
48. Borg, R.E.; Rochford, J. Molecular Photoacoustic Contrast Agents: Design Principles & Applications. *Photochem. Photobiol.* **2018**, *94*, 1175–1209. [[CrossRef](#)] [[PubMed](#)]
49. Perez-Rodriguez, R.; Haitjema, C.; Huang, Q.; Nam, K.H.; Bernardis, S.; Ke, A.; DeLisa, M.P. Envelope stress is a trigger of CRISPR RNA-mediated DNA silencing in *Escherichia coli*. *Mol. Microbiol.* **2011**, *79*, 584–599. [[CrossRef](#)]
50. Dolan, A.E.; Hou, Z.; Xiao, Y.; Gramelspacher, M.J.; Heo, J.; Howden, S.E.; Freddolino, P.L.; Ke, A.; Zhang, Y. Introducing a Spectrum of Long-Range Genomic Deletions in Human Embryonic Stem Cells Using Type I CRISPR-Cas. *Mol. Cell* **2019**, *74*, 936–950.e935. [[CrossRef](#)]
51. Hu, C.; Ni, D.; Nam, K.H.; Majumdar, S.; McLean, J.; Stahlberg, H.; Terns, M.P.; Ke, A. Allosteric control of type I-A CRISPR-Cas3 complexes and establishment as effective nucleic acid detection and human genome editing tools. *Mol. Cell* **2022**, *82*, 2754–2768.e2755. [[CrossRef](#)]
52. Tan, R.; Krueger, R.K.; Gramelspacher, M.J.; Zhou, X.; Xiao, Y.; Ke, A.; Hou, Z.; Zhang, Y. Cas11 enables genome engineering in human cells with compact CRISPR-Cas3 systems. *Mol. Cell* **2022**, *82*, 852–867.e855. [[CrossRef](#)]
53. Shimomura, O.; Johnson, F.H.; Saiga, Y. Extraction, Purification and Properties of Aequorin, a Bioluminescent Protein from the Luminous Hydromedusan, *Aequorea*. *J. Cell. Comp. Physiol.* **1962**, *59*, 223–239. [[CrossRef](#)]
54. Ormö, M.; Cubitt, A.B.; Kallio, K.; Gross, L.A.; Tsien, R.Y.; Remington, S.J. Crystal Structure of the *Aequorea victoria* Green Fluorescent Protein. *Science* **1996**, *273*, 1392–1395. [[CrossRef](#)]

55. Zimmer, M. Green fluorescent protein (GFP): Applications, structure, and related photophysical behavior. *Chem. Rev.* **2002**, *102*, 759–781. [[CrossRef](#)]
56. Bae, J.E.; Kim, I.J.; Nam, K.H. Disruption of the hydrogen bonding network determines the pH-induced non-fluorescent state of the fluorescent protein ZsYellow by protonation of Glu221. *Biochem. Biophys. Res. Commun.* **2017**, *493*, 562–567. [[CrossRef](#)]
57. Tomosugi, W.; Matsuda, T.; Tani, T.; Nemoto, T.; Kotera, I.; Saito, K.; Horikawa, K.; Nagai, T. An ultramarine fluorescent protein with increased photostability and pH insensitivity. *Nat. Methods* **2009**, *6*, 351–353. [[CrossRef](#)]
58. Mena, M.A.; Treynor, T.P.; Mayo, S.L.; Daugherty, P.S. Blue fluorescent proteins with enhanced brightness and photostability from a structurally targeted library. *Nat. Biotechnol.* **2006**, *24*, 1569–1571. [[CrossRef](#)]
59. Costantini, L.M.; Baloban, M.; Markwardt, M.L.; Rizzo, M.A.; Guo, F.; Verkhusha, V.V.; Snapp, E.L. A palette of fluorescent proteins optimized for diverse cellular environments. *Nat. Commun.* **2015**, *6*, 7670. [[CrossRef](#)]
60. Erard, M.; Fredj, A.; Pasquier, H.; Beltolngar, D.-B.; Bousmah, Y.; Derrien, V.; Vincent, P.; Merola, F. Minimum set of mutations needed to optimize cyan fluorescent proteins for live cell imaging. *Mol. Biosyst.* **2013**, *9*, 258–267. [[CrossRef](#)]
61. Rizzo, M.A.; Springer, G.H.; Granada, B.; Piston, D.W. An improved cyan fluorescent protein variant useful for FRET. *Nat. Biotechnol.* **2004**, *22*, 445–449. [[CrossRef](#)]
62. Nguyen, A.W.; Daugherty, P.S. Evolutionary optimization of fluorescent proteins for intracellular FRET. *Nat. Biotechnol.* **2005**, *23*, 355–360. [[CrossRef](#)]
63. Goedhart, J.; von Stetten, D.; Noirclerc-Savoye, M.; Lelimosin, M.; Joosen, L.; Hink, M.A.; van Weeren, L.; Gadella, T.W.J.; Royant, A. Structure-guided evolution of cyan fluorescent proteins towards a quantum yield of 93%. *Nat. Commun.* **2012**, *3*, 751. [[CrossRef](#)]
64. Zacharias, D.A.; Violin, J.D.; Newton, A.C.; Tsien, R.Y. Partitioning of Lipid-Modified Monomeric GFPs into Membrane Microdomains of Live Cells. *Science* **2002**, *296*, 913–916. [[CrossRef](#)]
65. Bajar, B.T.; Wang, E.S.; Lam, A.J.; Kim, B.B.; Jacobs, C.L.; Howe, E.S.; Davidson, M.W.; Lin, M.Z.; Chu, J. Improving brightness and photostability of green and red fluorescent proteins for live cell imaging and FRET reporting. *Sci. Rep.* **2016**, *6*, 20889. [[CrossRef](#)] [[PubMed](#)]
66. Shaner, N.C.; Lambert, G.G.; Chamma, A.; Ni, Y.; Cranfill, P.J.; Baird, M.A.; Sell, B.R.; Allen, J.R.; Day, R.N.; Israelsson, M.; et al. A bright monomeric green fluorescent protein derived from *Branchiostoma lanceolatum*. *Nat. Methods* **2013**, *10*, 407–409. [[CrossRef](#)] [[PubMed](#)]
67. Lee, J.; Liu, Z.; Suzuki, P.H.; Ahrens, J.F.; Lai, S.; Lu, X.; Guan, S.; St-Pierre, F. Versatile phenotype-activated cell sorting. *Sci. Adv.* **2020**, *6*, eabb7438. [[CrossRef](#)] [[PubMed](#)]
68. Kremers, G.-J.; Goedhart, J.; van Munster, E.B.; Gadella, T.W.J. Cyan and Yellow Super Fluorescent Proteins with Improved Brightness, Protein Folding, and FRET Förster Radius. *Biochemistry* **2006**, *45*, 6570–6580. [[CrossRef](#)]
69. Shaner, N.C.; Campbell, R.E.; Steinbach, P.A.; Giepmans, B.N.G.; Palmer, A.E.; Tsien, R.Y. Improved monomeric red, orange and yellow fluorescent proteins derived from *Discosoma* sp. red fluorescent protein. *Nat. Biotechnol.* **2004**, *22*, 1567–1572. [[CrossRef](#)]
70. Sakaue-Sawano, A.; Kurokawa, H.; Morimura, T.; Hanyu, A.; Hama, H.; Osawa, H.; Kashiwagi, S.; Fukami, K.; Miyata, T.; Miyoshi, H.; et al. Visualizing Spatiotemporal Dynamics of Multicellular Cell-Cycle Progression. *Cell* **2008**, *132*, 487–498. [[CrossRef](#)]
71. Merzlyak, E.M.; Goedhart, J.; Shcherbo, D.; Bulina, M.E.; Shcheglov, A.S.; Fradkov, A.F.; Gaintzeva, A.; Lukyanov, K.A.; Lukyanov, S.; Gadella, T.W.J.; et al. Bright monomeric red fluorescent protein with an extended fluorescence lifetime. *Nat. Methods* **2007**, *4*, 555–557. [[CrossRef](#)]
72. Shaner, N.C.; Lin, M.Z.; McKeown, M.R.; Steinbach, P.A.; Hazelwood, K.L.; Davidson, M.W.; Tsien, R.Y. Improving the photostability of bright monomeric orange and red fluorescent proteins. *Nat. Methods* **2008**, *5*, 545–551. [[CrossRef](#)]
73. Bindels, D.S.; Haarbosch, L.; van Weeren, L.; Postma, M.; Wiese, K.E.; Mastop, M.; Aumonier, S.; Gotthard, G.; Royant, A.; Hink, M.A.; et al. mScarlet: A bright monomeric red fluorescent protein for cellular imaging. *Nat. Methods* **2016**, *14*, 53–56. [[CrossRef](#)]
74. Nishizawa, K.; Kita, Y.; Kitayama, M.; Ishimoto, M. A red fluorescent protein, DsRed2, as a visual reporter for transient expression and stable transformation in soybean. *Plant Cell Rep.* **2006**, *25*, 1355–1361. [[CrossRef](#)]
75. Wang, L.; Jackson, W.C.; Steinbach, P.A.; Tsien, R.Y. Evolution of new nonantibody proteins via iterative somatic hypermutation. *Proc. Natl. Acad. Sci. USA* **2004**, *101*, 16745–16749. [[CrossRef](#)]
76. Lin, M.Z.; McKeown, M.R.; Ng, H.-L.; Aguilera, T.A.; Shaner, N.C.; Campbell, R.E.; Adams, S.R.; Gross, L.A.; Ma, W.; Alber, T.; et al. Autofluorescent Proteins with Excitation in the Optical Window for Intravital Imaging in Mammals. *Chem. Biol.* **2009**, *16*, 1169–1179. [[CrossRef](#)]
77. Morozova, K.S.; Piatkevich, K.D.; Gould, T.J.; Zhang, J.; Bewersdorf, J.; Verkhusha, V.V. Far-Red Fluorescent Protein Excitable with Red Lasers for Flow Cytometry and Superresolution STED Nanoscopy. *Biophys. J.* **2010**, *99*, L13–L15. [[CrossRef](#)]
78. Lambert, T.J. FPbase: A community-editable fluorescent protein database. *Nat. Methods* **2019**, *16*, 277–278. [[CrossRef](#)]
79. Kogure, T.; Karasawa, S.; Araki, T.; Saito, K.; Kinjo, M.; Miyawaki, A. A fluorescent variant of a protein from the stony coral *Montipora* facilitates dual-color single-laser fluorescence cross-correlation spectroscopy. *Nat. Biotechnol.* **2006**, *24*, 577–581. [[CrossRef](#)]
80. Piatkevich, K.D.; Hulit, J.; Subach, O.M.; Wu, B.; Abdulla, A.; Segall, J.E.; Verkhusha, V.V. Monomeric red fluorescent proteins with a large Stokes shift. *Proc. Natl. Acad. Sci. USA* **2010**, *107*, 5369–5374. [[CrossRef](#)]

81. Zapata-Hommer, O.; Griesbeck, O. Efficiently folding and circularly permuted variants of the Sapphire mutant of GFP. *BMC Biotechnol.* **2003**, *3*, 5. [[CrossRef](#)]
82. Gunewardene, M.S.; Subach, F.V.; Gould, T.J.; Penoncello, G.P.; Gudheti, M.V.; Verkhusha, V.V.; Hess, S.T. Superresolution Imaging of Multiple Fluorescent Proteins with Highly Overlapping Emission Spectra in Living Cells. *Biophys. J.* **2011**, *101*, 1522–1528. [[CrossRef](#)]
83. Subach, F.V.; Patterson, G.H.; Manley, S.; Gillette, J.M.; Lippincott-Schwartz, J.; Verkhusha, V.V. Photoactivatable mCherry for high-resolution two-color fluorescence microscopy. *Nat. Methods* **2009**, *6*, 153–159. [[CrossRef](#)]
84. Subach, F.V.; Patterson, G.H.; Renz, M.; Lippincott-Schwartz, J.; Verkhusha, V.V. Bright Monomeric Photoactivatable Red Fluorescent Protein for Two-Color Super-Resolution sptPALM of Live Cells. *J. Am. Chem. Soc.* **2010**, *132*, 6481–6491. [[CrossRef](#)]
85. Ando, R.; Mizuno, H.; Miyawaki, A. Regulated Fast Nucleocytoplasmic Shuttling Observed by Reversible Protein Highlighting. *Science* **2004**, *306*, 1370–1373. [[CrossRef](#)] [[PubMed](#)]
86. Chang, H.; Zhang, M.; Ji, W.; Chen, J.; Zhang, Y.; Liu, B.; Lu, J.; Zhang, J.; Xu, P.; Xu, T. A unique series of reversibly switchable fluorescent proteins with beneficial properties for various applications. *Proc. Natl. Acad. Sci. USA* **2012**, *109*, 4455–4460. [[CrossRef](#)] [[PubMed](#)]
87. Pletnev, S.; Subach, F.V.; Dauter, Z.; Wlodawer, A.; Verkhusha, V.V. A Structural Basis for Reversible Photoswitching of Absorbance Spectra in Red Fluorescent Protein rsTagRFP. *J. Mol. Biol.* **2012**, *417*, 144–151. [[CrossRef](#)] [[PubMed](#)]
88. Ando, R.; Hama, H.; Yamamoto-Hino, M.; Mizuno, H.; Miyawaki, A. An optical marker based on the UV-induced green-to-red photoconversion of a fluorescent protein. *Proc. Natl. Acad. Sci. USA* **2002**, *99*, 12651–12656. [[CrossRef](#)]
89. Zhang, M.; Chang, H.; Zhang, Y.; Yu, J.; Wu, L.; Ji, W.; Chen, J.; Liu, B.; Lu, J.; Liu, Y.; et al. Rational design of true monomeric and bright photoactivatable fluorescent proteins. *Nat. Methods* **2012**, *9*, 727–729. [[CrossRef](#)]
90. Labas, Y.A.; Gurskaya, N.G.; Yanushevich, Y.G.; Fradkov, A.F.; Lukyanov, K.A.; Lukyanov, S.A.; Matz, M.V. Diversity and evolution of the green fluorescent protein family. *Proc. Natl. Acad. Sci. USA* **2002**, *99*, 4256–4261. [[CrossRef](#)]
91. Miyawaki, A.; Llopis, J.; Heim, R.; McCaffery, J.M.; Adams, J.A.; Ikura, M.; Tsien, R.Y. Fluorescent indicators for Ca²⁺ based on green fluorescent proteins and calmodulin. *Nature* **1997**, *388*, 882–887. [[CrossRef](#)]
92. Kim, I.J.; Xu, Y.; Nam, K.H. Spectroscopic and Structural Analysis of Cu²⁺-Induced Fluorescence Quenching of ZsYellow. *Biosensors* **2020**, *10*, 29. [[CrossRef](#)]
93. Kim, I.J.; Xu, Y.; Nam, K.H. Metal-Induced Fluorescence Quenching of Photoconvertible Fluorescent Protein DendFP. *Molecules* **2022**, *27*, 2922. [[CrossRef](#)]
94. Isarankura-Na-Ayudhya, C.; Tantimongcolwat, T.; Galla, H.J.; Prachayasittikul, V. Fluorescent protein-based optical biosensor for copper ion quantitation. *Biol. Trace Elem. Res.* **2010**, *134*, 352–363. [[CrossRef](#)]
95. Richmond, T.A.; Takahashi, T.T.; Shimkhada, R.; Bernsdorf, J. Engineered metal binding sites on green fluorescence protein. *Biochem. Biophys. Res. Commun.* **2000**, *268*, 462–465. [[CrossRef](#)]
96. Mizuno, T.; Muraio, K.; Tanabe, Y.; Oda, M.; Tanaka, T. Metal-ion-dependent GFP emission in vivo by combining a circularly permuted green fluorescent protein with an engineered metal-ion-binding coiled-coil. *J. Am. Chem. Soc.* **2007**, *129*, 11378–11383. [[CrossRef](#)]
97. Eli, P.; Chakrabartty, A. Variants of DsRed fluorescent protein: Development of a copper sensor. *Protein Sci.* **2006**, *15*, 2442–2447. [[CrossRef](#)]
98. Kim, I.J.; Kim, S.; Park, J.; Eom, I.; Kim, S.; Kim, J.H.; Ha, S.C.; Kim, Y.G.; Hwang, K.Y.; Nam, K.H. Crystal structures of Dronpa complexed with quenchable metal ions provide insight into metal biosensor development. *FEBS Lett.* **2016**, *590*, 2982–2990. [[CrossRef](#)]
99. Bae, J.E.; Kim, I.J.; Nam, K.H. Spectroscopic Analysis of the Cu²⁺-Induced Fluorescence Quenching of Fluorescent Proteins AmCyan and mOrange2. *Mol. Biotechnol.* **2018**, *60*, 485–491. [[CrossRef](#)]
100. Kim, I.J.; Xu, Y.; Nam, K.H. Spectroscopic Analysis of Fe Ion-Induced Fluorescence Quenching of the Green Fluorescent Protein ZsGreen. *J. Fluoresc.* **2021**, *31*, 307–314. [[CrossRef](#)]
101. Matz, M.V.; Fradkov, A.F.; Labas, Y.A.; Savitsky, A.P.; Zaraisky, A.G.; Markelov, M.L.; Lukyanov, S.A. Fluorescent proteins from nonbioluminescent Anthozoa species. *Nat. Biotechnol.* **1999**, *17*, 969–973. [[CrossRef](#)]
102. Sumner, J.P.; Westerberg, N.M.; Stoddard, A.K.; Hurst, T.K.; Cramer, M.; Thompson, R.B.; Fierke, C.A.; Kopelman, R. DsRed as a highly sensitive, selective, and reversible fluorescence-based biosensor for both Cu⁺ and Cu²⁺ ions. *Biosens. Bioelectron.* **2006**, *21*, 1302–1308. [[CrossRef](#)]
103. Rahimi, Y.; Goulding, A.; Shrestha, S.; Mirpuri, S.; Deo, S.K. Mechanism of copper induced fluorescence quenching of red fluorescent protein, DsRed. *Biochem. Biophys. Res. Commun.* **2008**, *370*, 57–61. [[CrossRef](#)]
104. Yarbrough, D.; Wachter, R.M.; Kallio, K.; Matz, M.V.; Remington, S.J. Refined crystal structure of DsRed, a red fluorescent protein from coral, at 2.0-Å resolution. *Proc. Natl. Acad. Sci. USA* **2001**, *98*, 462–467. [[CrossRef](#)]
105. Taraska, J.W.; Puljung, M.C.; Olivier, N.B.; Flynn, G.E.; Zagotta, W.N. Mapping the structure and conformational movements of proteins with transition metal ion FRET. *Nat. Methods* **2009**, *6*, 532–537. [[CrossRef](#)] [[PubMed](#)]
106. Nam, K.H.; Kwon, O.Y.; Sugiyama, K.; Lee, W.H.; Kim, Y.K.; Song, H.K.; Kim, E.E.; Park, S.Y.; Jeon, H.; Hwang, K.Y. Structural characterization of the photoswitchable fluorescent protein Dronpa-C62S. *Biochem. Biophys. Res. Commun.* **2007**, *354*, 962–967. [[CrossRef](#)] [[PubMed](#)]

107. Guryev, O.; Jaimes, M.C.; Edinger, M.G.; Matvienko, M.; Abrams, B.; Dubrovsky, T. Use of a new violet-excitable AmCyan variant as a label in cell analysis. *Cytom. Part A* **2012**, *81A*, 627–634. [[CrossRef](#)] [[PubMed](#)]
108. Remington, S.J.; Wachter, R.M.; Yarbrough, D.K.; Branchaud, B.; Anderson, D.C.; Kallio, K.; Lukyanov, K.A. zFP538, a yellow-fluorescent protein from *Zoanthus*, contains a novel three-ring chromophore. *Biochemistry* **2005**, *44*, 202–212. [[CrossRef](#)] [[PubMed](#)]
109. Wenck, A.; Pugieux, C.; Turner, M.; Dunn, M.; Stacy, C.; Tiozzo, A.; Dunder, E.; van Grinsven, E.; Khan, R.; Sigareva, M.; et al. Reef-coral proteins as visual, non-destructive reporters for plant transformation. *Plant Cell Rep.* **2003**, *22*, 244–251. [[CrossRef](#)]
110. Pletneva, N.V.; Pletnev, S.; Pakhomov, A.A.; Chertkova, R.V.; Martynov, V.I.; Muslinkina, L.; Dauter, Z.; Pletnev, V.Z. Crystal structure of the fluorescent protein from *Dendronephthya* sp. in both green and photoconverted red forms. *Acta Crystallogr. D Struct. Biol.* **2016**, *72*, 922–932. [[CrossRef](#)]
111. Pakhomov, A.A.; Chertkova, R.V.; Martynov, V.I. Ph-Sensor Properties of a Fluorescent Protein from *Dendronephthya* sp. *Bioorg. Khim.* **2015**, *41*, 669–674. [[CrossRef](#)]
112. Brown, D.R.; Qin, K.; Herms, J.W.; Madlung, A.; Manson, J.; Strome, R.; Fraser, P.E.; Kruck, T.; von Bohlen, A.; Schulz-Schaeffer, W.; et al. The cellular prion protein binds copper in vivo. *Nature* **1997**, *390*, 684–687. [[CrossRef](#)]
113. Atwood, C.S.; Moir, R.D.; Huang, X.; Scarpa, R.C.; Bacarra, N.M.E.; Romano, D.M.; Hartshorn, M.A.; Tanzi, R.E.; Bush, A.I. Dramatic Aggregation of Alzheimer A β by Cu(II) Is Induced by Conditions Representing Physiological Acidosis. *J. Biol. Chem.* **1998**, *273*, 12817–12826. [[CrossRef](#)]
114. Cherny, R.A.; Atwood, C.S.; Xilinas, M.E.; Gray, D.N.; Jones, W.D.; McLean, C.A.; Barnham, K.J.; Volitakis, I.; Fraser, F.W.; Kim, Y.-S.; et al. Treatment with a Copper-Zinc Chelator Markedly and Rapidly Inhibits β -Amyloid Accumulation in Alzheimer's Disease Transgenic Mice. *Neuron* **2001**, *30*, 665–676. [[CrossRef](#)]
115. Qin, K.; Yang, Y.; Mastrangelo, P.; Westaway, D. Mapping Cu(II) Binding Sites in Prion Proteins by Diethyl Pyrocarbonate Modification and Matrix-assisted Laser Desorption Ionization-Time of Flight (MALDI-TOF) Mass Spectrometric Footprinting. *J. Biol. Chem.* **2002**, *277*, 1981–1990. [[CrossRef](#)]
116. Huang, A.; Li, W.; Shi, S.; Yao, T. Quantitative Fluorescence Quenching on Antibody-conjugated Graphene Oxide as a Platform for Protein Sensing. *Sci. Rep.* **2017**, *7*, 40772. [[CrossRef](#)]
117. Zhao, H.; Zastrow, M.L. Transition Metals Induce Quenching of Monomeric Near-Infrared Fluorescent Proteins. *Biochemistry* **2022**, *61*, 494–504. [[CrossRef](#)]

Disclaimer/Publisher's Note: The statements, opinions and data contained in all publications are solely those of the individual author(s) and contributor(s) and not of MDPI and/or the editor(s). MDPI and/or the editor(s) disclaim responsibility for any injury to people or property resulting from any ideas, methods, instructions or products referred to in the content.